Hindawi Publishing Corporation
International Journal of Electrochemistry
Volume 2012, Article ID 475417, 10 pages
doi:10.1155/2012/475417

Research Article

Spontaneous Synthesis and Electrochemical Characterization of Nanostructured MnO_2 on Nitrogen-Incorporated Carbon Nanotubes

Ying-Chu Chen,[1,2] Yu-Kuei Hsu,[3] Yan-Gu Lin,[4] Li-Chyong Chen,[1] and Kuei-Hsien Chen[1,4]

[1] *Center for Condensed Matter Sciences, National Taiwan University, Taipei 106, Taiwan*
[2] *Department of Chemical Engineering, National Taiwan University, Taipei 106, Taiwan*
[3] *Department of Opto-Electronic Engineering, National Dong Hwa University, Hualien 97401, Taiwan*
[4] *Institute of Atomic and Molecular Science, Academia Sinica, Taipei 106, Taiwan*

Correspondence should be addressed to Li-Chyong Chen, chenlc@ntu.edu.tw
and Kuei-Hsien Chen, chenkh@pub.iams.sinica.edu.tw

Received 2 September 2011; Accepted 11 October 2011

Academic Editor: V. S. Reddy Channu

This paper investigated the layered manganese dioxide with hydrate ($MnO_2 \cdot xH_2O$) deposits onto nitrogen-containing carbon nanotube (CNxNTs) as a hierarchical electrode for an energy-storage device. The dense and entangled CNxNTs were directly grown by microwave plasma-enhanced chemical vapor deposition (MPECVD) on a carbon cloth (CC), and subsequently used as a current collector. By controlling the pH value of $KMnO_4$ precursor solution, and incorporating nitrogen into CNTs as a reducing agent, the MnO_2 thin layer was uniformly fabricated on the CNxNTs at room temperature by using a spontaneous reduction method. The role of incorporation nitrogen is not only capable of creating active sites on the CNT surface, but can also donate electrons to reduce MnO_4^- to MnO_2 spontaneously. From the measurements of cyclic voltammograms and galvanostatic charge/discharge, MnO_2/CNxNTs/CC composite electrodes illustrated excellent specific capacitance of 589.1 Fg^{-1}. The key factor for high performance could be attributed to the thin-layered MnO_2 nanostructure, which resulted in the full utilization of MnO_2 deposits. Hence, the hierarchically porous MnO_2/CNxNTs/CC electrodes exhibited excellent capacitive behavior for electrochemical capacitor application.

1. Introduction

Electrochemical capacitors, commonly referred to as supercapacitors, combine the advantages of both conventional capacitors and rechargeable batteries. The high storage of electron energy and fast delivery of power within a short time make supercapacitors complementary charge-storage devices to renewable energy production devices, such as solar cells and fuel cells [1–6]. Various studies have focused on supercapacitors because of their potential application as energy storage devices in the applications of hybrid electric vehicles and short-term power sources for portable and flexible electronic devices [4–6].

According to the energy storage mechanism, supercapacitors can be divided into two categories, as follows: electrochemical double-layer capacitors (EDLCs) and pseudocapacitors. The EDLCs are chiefly composed of carbon-based materials with high specific surface area, such as activated carbon, carbon nanotubes, and graphene [7–9]. The electron energy is reserved through the rapid ions adsorption/desorption at the interface between electrode and electrolyte, where the capacitance arises from electrostatic separation at this interface. The electrode materials for pseudocapacitors include electrochemically active materials with several redox states or structures, such as transition metal oxides (e.g., oxides of Ru, Ni, Sn, and Mn) and electronically conducting polymers [10–15]. In pseudocapacitors, the electron storage mechanism involves reversible Faradaic reaction, which means that the bulk material can be used for energy stock. Therefore, the capacitive performance is expected to be higher than that of EDLCs.

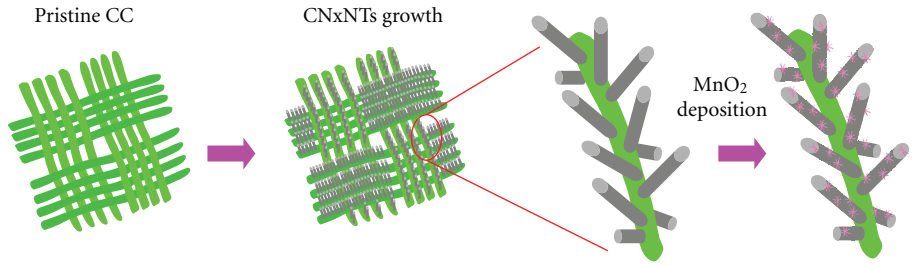

Figure 1: (a) Schematic diagram for fabrication of MnO_2/CNxNTs/CC hybrid electrode.

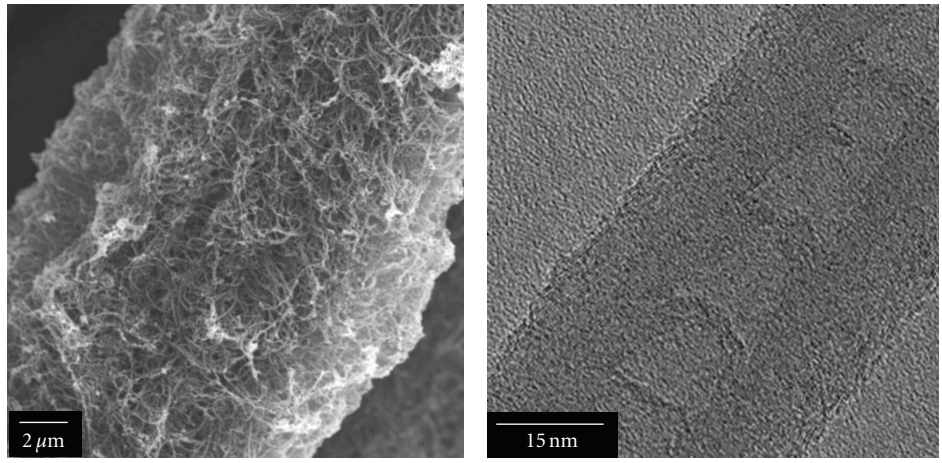

(a) (b)

Figure 2: (a) FESEM images of pristine CNxNTs/CC current collector and (b) high-resolution TEM images of the Ni-catalyzed CNxNTs with bamboo-like structure.

Among the materials for pseudocapacitors, hydrous manganese dioxide ($MnO_2 \cdot xH_2O$), as the electrode of a supercapacitor has recently attracted attention because of its high theoretical capacitance (~1380 Fg^{-1}), environmentally friendly nature, promising electrochemical performance, and the low cost of raw material [14–19]. However, in the literature the specific capacitance of MnO_2 was typically restricted to 200~300 Fg^{-1} [14–17] because of its intrinsically poor electronic conductivity and dense morphology. To overcome these problems, recent investigations have highlighted the influence of the nanostructure of the electrode on the electrochemical performance for the effective utilization of active material [16–19]. Some literatures have demonstrated the enhancement of specific capacitance by adopting the highly porous microstructure composite electrode [20]. Therefore, in the design of a composite electrode, it is ideal to fabricate an extremely thin layer (~nm) of nanostructured MnO_2 onto the current collector, controlling the coating layer thickness and uniform surface coverage to reach the high theoretical specific capacitance. To achieve this goal, the direct-growing nitrogen-incorporated carbon nanotubes (CNxNTs) on the carbon cloth (CC) function as a hierarchical current collector, which is used to improve electronic conductivity and increase specific surface area [21, 22]. Due to the incorporation of nitrogen, CNxNTs also inherently possess surface defects, creating a further increase of anchoring sites for uniform deposition of MnO_2 nanostructure, and facilitating the charge-transfer between active materials and CNxNTs. Hence, in this study, the entangled and direct-grown CNxNTs were fabricated via microwave plasma-enhanced chemical vapor deposition (MPECVD), and subsequent deposition of MnO_2 on CNxNTs surface by using the spontaneous reduction method was further constructed as the hierarchical electrode. The prepared MnO_2/CNxNTs/CC composite, with a nanometer-scale MnO_2 layer, is expected to exhibit excellent specific capacitance resulting from the large surface-to-volume ratio, high stability, and high-rate capability.

2. Experimental Section

2.1. Preparation of CNxNTs/CC Current Collector. To further extend our previous result, the nitrogen-containing carbon nanotubes (CNxNTs) were directly grown on a commercially available CC (E-TEK, USA), with specifications as follows: B-1 Designation A (weave = plain; weight = 116 g/m^2; thickness = 0.35 mm; 0 wt. % wet proofing), and the entire composite was used as the current collector. The detailed procedure for direct growth of CNxNTs can be found elsewhere [23], but is described here briefly. The CNxNTs/CC composite was prepared by nickel-catalyst-assisted MPECVD technique. First, nickel, as catalysts for CNxNTs growth, were electrochemically deposited onto CC in an electrolyte solution of 0.1 M H_2SO_4 + 0.1 M $NiSO_4$ under a galvanostatic

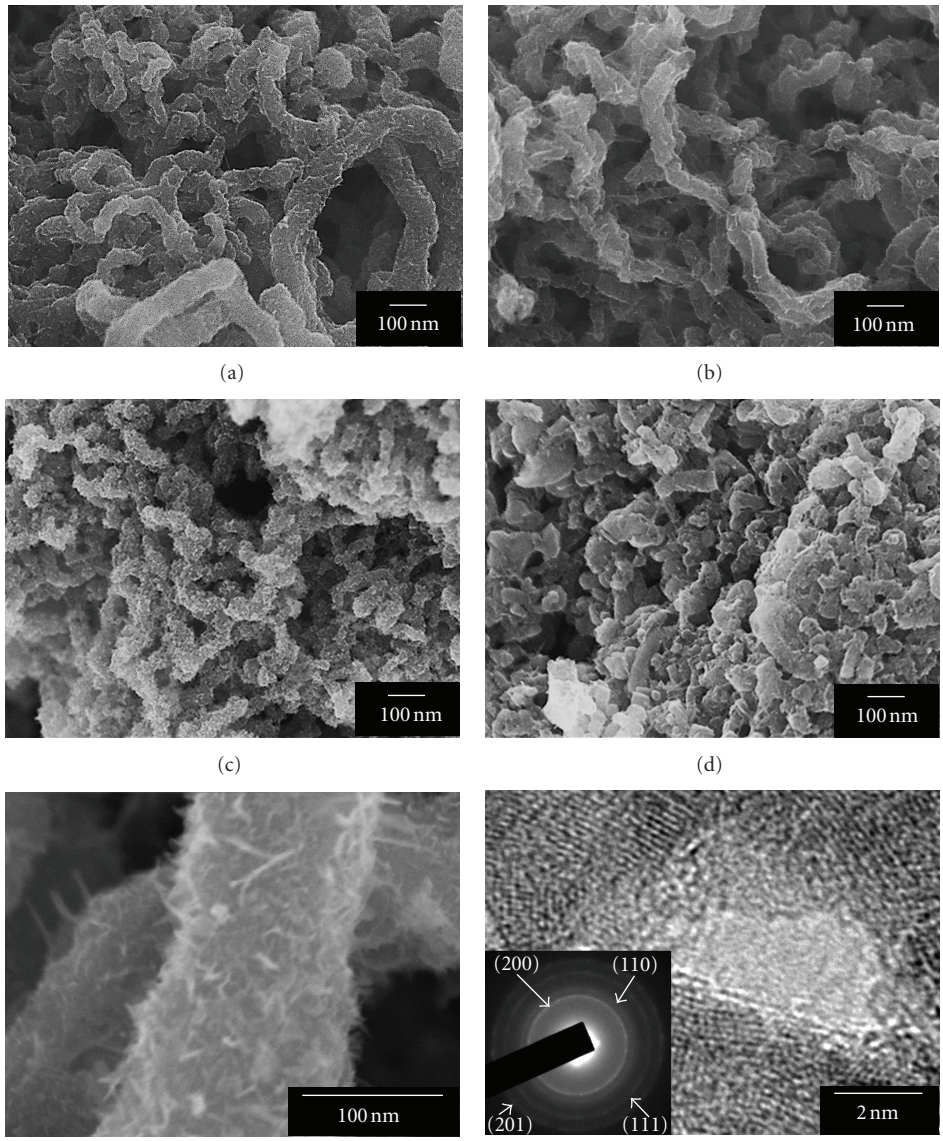

Figure 3: FESEM micrographs of MnO_2/CNxNTs/CC hybrid electrodes, fabricated via spontaneous reduction, for different deposition time (a)–(d) low magnification, (e) high magnification. (f) HRTEM images and the corresponding selected area electron diffraction pattern of MnO_2.

condition of 0.5 mA cm^{-2} for durations of 500 s. Prior to the growth of CNxNTs, the nickel-coated CC was subjected to hydrogen-plasma treatment of the catalyst at a microwave power of 1 kW, under chamber pressure 28 torr for 10 min. Subsequently, the synthesis of CNxNTs was conducted in a mixture of precursors ($CH_4/H_2/N_2$ = 20 : 80 : 80) at a microwave power of 2 kW, under a chamber pressure of 40 torr and a substrate temperature of 900°C for a growth duration of 10 min.

2.2. Preparation of MnO_2/CNxNTs/CC Composite Electrode. The spontaneous reduction method was used to fabricate the composite electrode [24]. The prepared CNxNTs/CC electrode was immersed into the precursor of 0.1 M $KMnO_4$ solution to deposit the MnO_2 for different reaction times, from 50 min to 250 min. The pH of 0.1 M $KMnO_4$ solution was adjusted to neutral by 0.01 M H_2SO_4 solution. The MnO_2 was directly deposited onto the CNxNTs surface via a spontaneous reduction between the CNxNTs and MnO_4^-. Once the deposition process was completed, the CNxNTs/CC electrode with the deposits was rinsed with distilled water, and subsequently dried at room temperature for further analysis. All the chemicals used for MnO_2 deposition (H_2SO_4, $KMnO_4$) were of analytical-reagent grade from Aldrich. Double-distilled water was used throughout the process.

2.3. Characterization of MnO_2/CNxNTs/CC Composite Electrode. The morphologic and structural evolution, with different reaction times of composite electrode, was

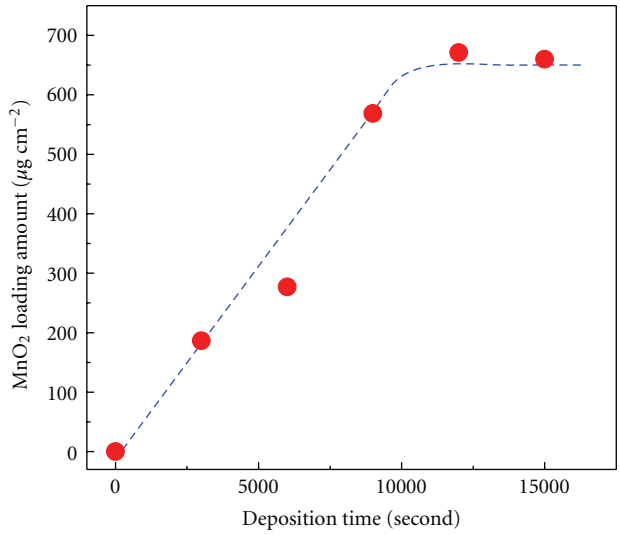

Figure 4: Variation in loading amount of MnO_2/CNxNTs/CC hybrid electrodes for different deposition time. (Loading amount measured using ICP-OES).

investigated by field-emission scanning electron microscopy (FESEM, JEOL-6700), high-resolution transmission electron microscope (HRTEM, JEOL-400 EX), X-ray photoemission spectroscopy (Microlab 350 XPS), and Raman spectroscopy (Jobin-Yvon LabRAM HR800). Electrochemical measurements were conducted using Solartron electrochemical test system (1470E) at ambient temperature. The capacitive properties of the composite electrode were investigated by cyclic voltammetry (CV) and galvanostatic charge-discharge method, in 0.1 M Na_2SO_4 aqueous solution as the electrolyte by using a conventional three-electrode system. The MnO_2/CNxNTs/CC composite, with a definite area of 1 × 1 cm^2, was used as the working electrode. A platinum foil served as the counter electrode, and an Ag/AgCl (3 M KCl, 0.207 V versus SHE) reference electrode was used to control the potential of the working electrode. All electrochemical experiments were conducted at room temperature, and all potential values refer to an Ag/AgCl reference electrode. The mass per unit area of the active materials was determined by inductively coupled plasma-optical emission spectroscopy (ICP-OES, PerkinElmer ICP-OES Optima 125 3000).

3. Results and Discussion

3.1. Morphology. The preparation procedure for MnO_2/CNxNTs/CC composite electrode is illustrated schematically in Figure 1. First, the entangled network of CNxNTs with high surface area, which facilitates the transportation of ions from bulk solution to electrode surface, was fabricated onto a carbon fiber surface via MPECVD [25]. The spontaneous reduction method, using $KMnO_4$ aqueous solution as a precursor, was subsequently employed to deposit thin-layered MnO_2 nanostructures on CNxNTs. This MnO_2/CNxNTs/CC nanocomposite electrode, with binder-free and rapid electron transfer, benefits capacitive characteristics. Figure 2(a) displays the SEM image of the as-grown CNxNTs/CC composite as the current collector. Each of the carbon fibers was uniformly covered by the dense and entangled CNxNTs with narrow diameter distribution ranging from 40 to 60 nm (48 nm in average). This hierarchical nanostructure enabled us to further increase the surface area compared to naked carbon cloth, as well as the pore distribution, which facilitated the access of the ion. According to the image of HRTEM, as shown in Figure 2(b), all the CNxNTs are multiwalled and have typical "bamboo-like" compartments. The substitutional nitrogen doping can drastically modify the morphology of CNxNTs by introducing a number of pentagons and heptagons into the graphitic layers. The *d*-spacing was determined to be 0.342 nm, which is the spacing between the (002) crystalline planes of graphite.

The conformal deposition of MnO_2 was performed by using the spontaneous reduction method at room temperature, by controlling the deposition time for adjusting layer thickness. Figures 3(a)–3(d) shows the SEM images of the MnO_2/CNxNTs/CC composite at different deposition times from 50 min to 250 min, respectively. After MnO_2 deposition, the CNxNTs diameter grew slightly thicker, and the pore volume between each tube gradually decreased with increasing deposition time. The MnO_2/CNxNTs/CC, with a deposition time of 50 min, as shown in Figure 3(a), formed a core-shell structure, with a diameter of approximately 70 nm while an aggregation appeared at the deposition time of 250 min as illustrated in Figure 3(d). The aggregation of MnO_2, which would block the insertion of cations, indicates inferior capacitive behavior. At a deposition time below 250 min, uniform and floccule-like MnO_2 deposits can be observed on the CNxNTs in the high-magnification SEM image of Figure 3(e), which results in an apparent roughness of the MnO_2/CNxNTs hybrid electrode, compared to the pristine CNTs. In consideration to the diffusion length of cations, the thickness of MnO_2 film should be controlled to less than 150 nm (Figure 3(e)), which utilized ion insertion/desertion more efficiently, and could result in a higher

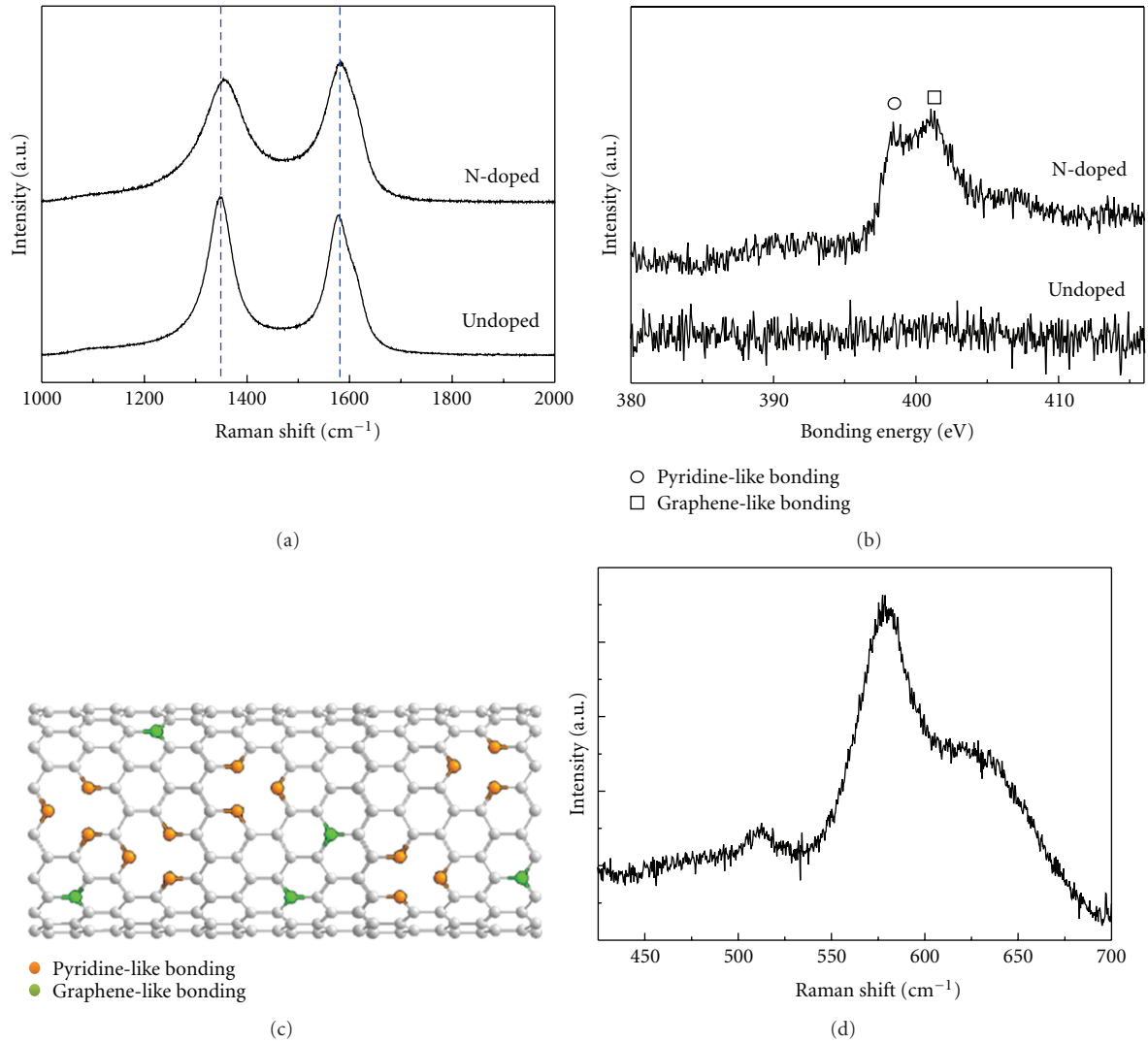

Figure 5: (a) Raman spectra and (b) XPS spectra of N 1s core level of CNxNTs/CC composite current collector. (c) Raman spectra of MnO_2/CNxNTs/CC hybrid electrode (deposition time of 150 min). (d) Raman spectra of MnO_2/CC hybrid electrode (deposition time of 150 min).

specific capacitance. TEM micrographs and corresponding selected area electron diffraction pattern (SAED), as shown in Figure 3(f), were taken from the MnO_2/CNxNTs/CC composite. According to the TEM image, the layered structure was composed of several petal-shaped thin nanosheets. Continuous ring pattern of SAED also confirmed their nanocrystalline nature. The *d*-spacings of (200), (110), (111), and (201), measured from the SAED pattern, are consistent with Birnessite-type MnO_2 (JCPDS 42–1317). ICP-MS was utilized to determine the loading amount of MnO_2 on the CNxNTs/CC current collector, as illustrated in Figure 4. The loading amount of MnO_2 linearly increased with extending deposition time. After the deposition time exceeds 150 min, the saturation of the loading amount, accompanied by apparent aggregation, can be observed, which is consistent with the SEM findings. When the loading mass reaches 0.65 mg cm^{-2}, there are no sufficient surface sites for deposition, and therefore, results in accumulation. This implied that the limitation of the loading amount was significantly dependent on the surface area of the carbon support. The loading level of the active materials was found to be approximately 0.2–0.7 mg cm^{-2}.

3.2. Structural Characterization and Composition Analysis. Figure 5(a) demonstrates the effect of Raman spectra of N dopant on CNxNTs. The 1350 cm^{-1} peak (D band) corresponds to the disorder-induced character because of the finite particle size effect or lattice distortion while the 1580 cm^{-1} peak (G band) corresponds to the in-plane stretching vibration mode E_{2g} of single crystal graphite [26]. These two characteristic peaks show some blue shift toward a higher wave number after the N incorporation. The factor could be ascribed to the tensile stress caused by the N-doping process. The intensity ratio of I_D/I_G increased with N decoration, which also exhibits raised defect density [27]. XPS was applied for reaching deeper into the electronic

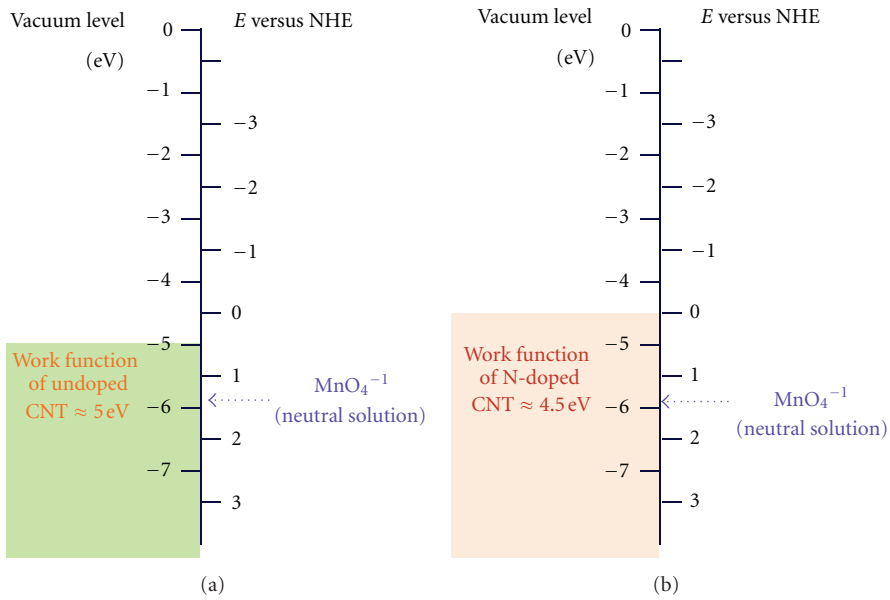

Figure 6: Energy diagram between the (a) Undoped CNTs and (b) N-doped CNTs and the $KMnO_4$ solution.

structures of CNxNTs, as illustrated in Figure 5(b). The N 1s XPS spectrum shows two characteristic peaks after N incorporation, compared to that of undoped CNTs, with no evident peaks. The peak located at 398.1 eV is assigned to tetrahedral nitrogen bonding within a substitutional pyridine-like dopant structure, and another peak, located at 400.8 eV, corresponds to trigonal nitrogen bonding within a graphene-like dopant structure [21, 23, 28–30]. The graphene and pyridine-like defects in the CNxNTs are shown in Figure 5(c). Hence, the resultant XPS spectra indicate that the N atoms were successfully doped into CNTs to form a chemical bonding. Figure 5(d) shows the Raman spectrum of MnO_2/CNxNTs/CC composited electrode, which was synthesized by using the spontaneous reduction method. Three major features for birnessite-type MnO_2 can be observed at 506, 575, and 640 cm^{-1} [31]. The Raman band at 640 cm^{-1} can be considered the symmetric stretching vibration (Mn–O) of the MnO_6 groups. The band located at 575 cm^{-1} is usually attributed to the (Mn–O) stretching vibration in the basal plane of the MnO_6 sheet. All the nanocomposites have the similar Raman spectra of the birnessite-type MnO_2, which confirms that MnO_2 successfully precipitated onto the CNxNTs.

3.3. Spontaneous Reduction Mechanism. The utilization of spontaneous reduction method for anchoring heteroatom on CNTs sidewall principally dominates by the difference between reduction potential of ion and work function of CNTs [32]. Using this technique, Ma et al. [24] in 2007 demonstrated the fabrication of MnO_2/CNTs, while CNTs acted as a reducing agent in the solution containing MnO_4^- ions. However, the slow kinetic reaction resulted in the requirement of a long reaction time and a high reaction temperature. To improve the slow kinetics, the N-doping technique can create a number of graphene and pyridine-like defects as anchoring sites on the surface of CNxNTs. These preferential defect sites also generate the hydrophilic interfaces on the sidewalls of CNxNTs, resulting in the rapid reaction between CNxNTs and MnO_2 deposit. In addition, CNxNTs exhibited a metallic behavior because of the N dopant as the electron donor. Therefore, the work function of CNxNTs can be further reduced in comparison to that of pure CNTs, which provides an even higher energy difference to raise the reduction rate. A detailed energy diagram, as shown in Figure 6, was demonstrated to explain the reaction mechanism. The left-hand side of the diagram is the work function (eV) of CNT, and the right-hand side is the reaction potential (V versus NHE) of MnO_4^- precursor solution,

$$MnO_4^{-1} + 2H_2O + 3e^- \longrightarrow MnO_2 + 4OH^- \quad (1)$$
$$E^o_{red} = +1.23\ V \text{ (versus NHE)} \quad \text{(Neutral medium)}$$

Typically, the work function of CNTs can be reduced from ~5 eV to ~4.5 eV after N incorporation [33]. The potential difference between the work function of CNTs and the reduction potential of MnO_4^- ions can significantly enhance 70% of the reduction power. These features of CNxNTs enable us to raise the kinetic reaction of MnO_2 deposit during the spontaneous reduction process. Furthermore, this enhancement of reduction power can rapidly force the reaction at room temperature. This spontaneous reduction technique, using novel properties of the N-doped CNTs, yields a promising route for fabricating the nanocomposite electrode in various applications.

3.4. Capacitive Properties. The electrochemical behavior of MnO_2/CNxNTs/CC composite electrodes, with different MnO_2 deposition times, was characterized by CV in 0.1 M Na_2SO_4 aqueous solutions at a scan rate of 10 mVs^{-1} under

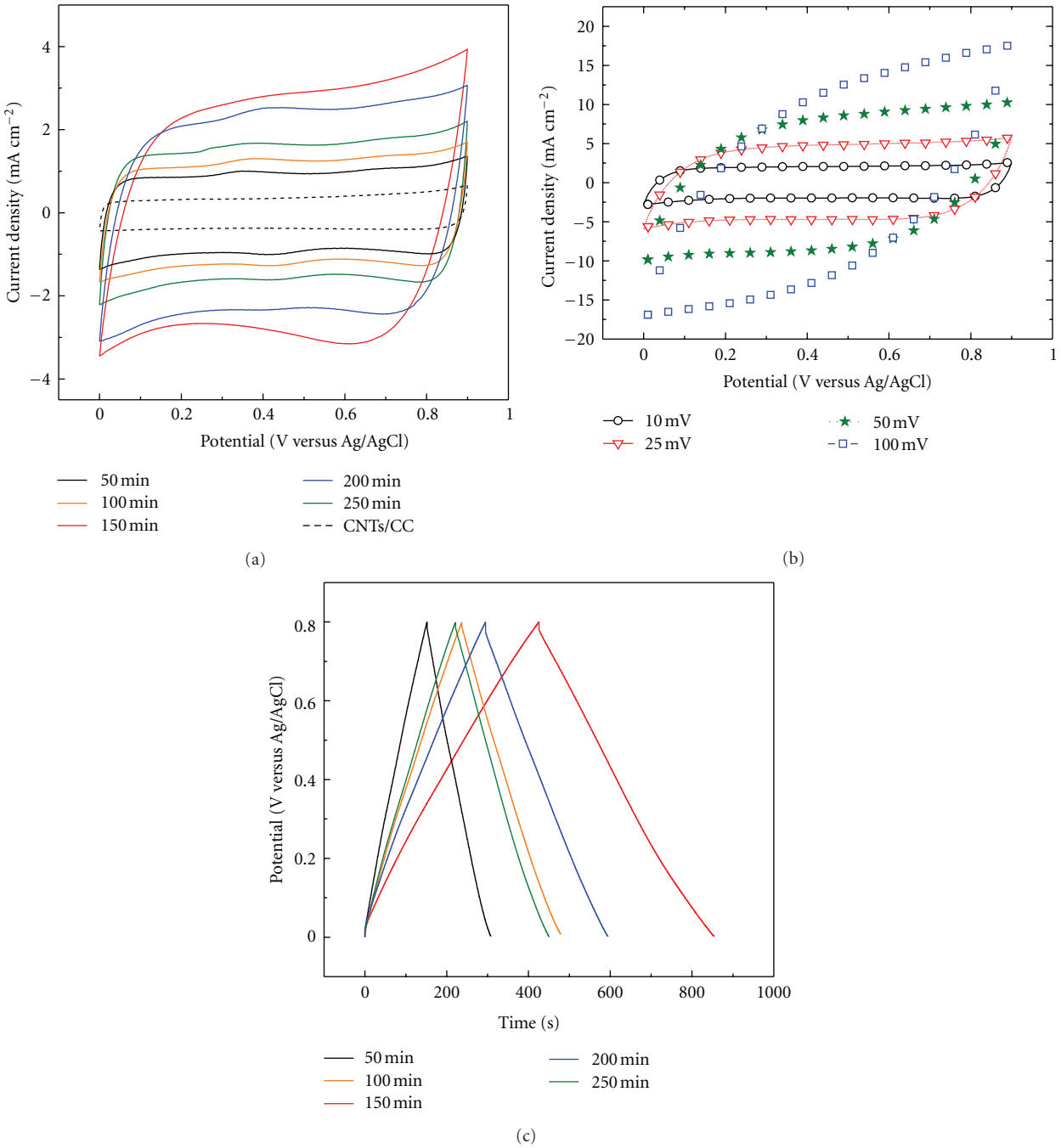

FIGURE 7: (a) Cyclic voltammograms of MnO_2/CNxNTs/CC hybrid electrodes with different deposition times at a scan rate of 10 mV/s; (b) cyclic voltammograms of the hybrid electrode under different scan rate of 10 mVs^{-1}, 25 mVs^{-1}, 50 mVs^{-1}, and 100 mVs^{-1}. (c) Galvonastatic charge-discharge curves of MnO_2/CNxNTs/CC hybrid electrodes with different deposition times at a fixed current density of 1.32 A/g.

a potential range from 0 to 0.9 V, as shown in Figure 7(a). For comparison, the black-dot CV curve presents a typical double-layer capacitive behavior of CNxNTs/CC electrode, of which the current density is approximately ~0.4 mA cm^{-2}. The current densities of MnO_2/CNxNTs/CC composite electrodes are always higher than that of CNxNTs/CC electrode, implying the origination of capacitive contribution from the MnO_2 layer. All the CV curves of MnO_2/CNxNTs/CC composite electrodes have a rectangular shape and symmetric feature, which indicate an ideal capacitive behavior. The curves with increasing deposition time show a tendency toward a higher current density in CV which can be attributed to the increase of MnO_2 deposits. However, when the deposition time exceeds 150 min, a further increase of MnO_2 deposit shows an inverse tendency toward less current density. The reason resulted from a thicker film and even the formation of aggregation, which was confirmed by SEM results. At a deposition time of 150 min, the high current

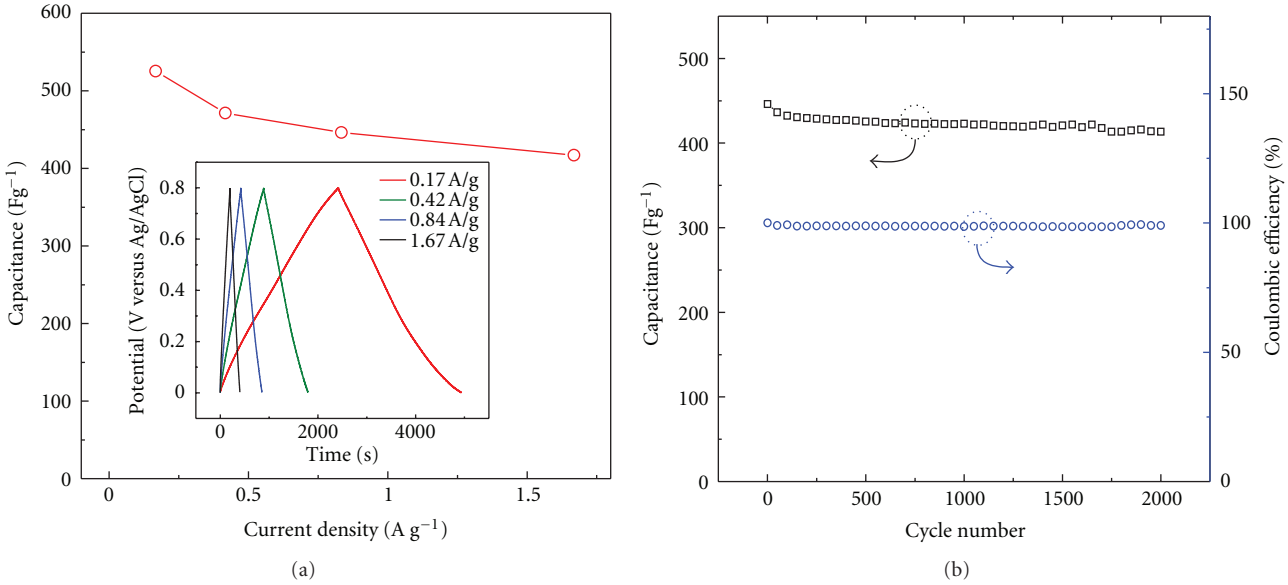

FIGURE 8: (a) Variation in gravimetric capacitance of MnO_2/CNxNTs/CC hybrid electrode (deposition time of 150 min) with different current density and the inset is the corresponding charge-discharge curves. (b) Cycle life of MnO_2/CNxNTs/CC supercapacitor.

density of the MnO_2/CNxNTs/CC composite electrode was attributed to the uniform covering of nanostructured MnO_2 and the high surface area of CNxNTs. Such a hierarchical composite electrode with high surface area can provide more superficial redox reaction within the interface between the electrode and electrolyte, which contribute to the high capacitance of the composite electrode [34]. Besides, the thin-layered MnO_2 further shortened the ionic transfer path, resulting in the full utilization of MnO_2 deposits. The CNxNTs with high electric conductivity also serve as a pathway for electron transfer, which advances the capacitive performance of the composite electrode. Consequently, the MnO_2/CNxNTs composite electrode can reasonably sustain the shape from higher to lower scan rate which indicates that this hybrid electrode has significant charge and discharge efficiency, as shown in Figure 7(b).

Figure 7(c) displays the galvanostatic charge/discharge plots of MnO_2/CNxNTs/CC composite electrodes at different deposition times. The symmetric anodic charging and cathodic discharging current reveal excellent electrochemical reversibility, which is consistent with CV observations. The specific capacitance of the electrode was calculated from the charge/discharge profile by using the following equation:

$$C_s = \frac{I \times t}{\Delta V \times m}, \tag{2}$$

where C_s (Fg^{-1}) is the specific capacitance of the electrode; t (s) is the discharge time; ΔV (V) is the potential window where the operation processes; I (A g^{-1}) is the applied current density based on the total electrode material. The specific capacitance values of MnO_2/CNxNTs/CC composite electrode evaluated from the discharge curves are 583.1, 510.7, 520, 410, and 270.6 Fg^{-1} at the deposition times of 50, 100, 150, 200, and 250 min, respectively. A specific capacitance as high as 589.1 Fg^{-1} implies that the capacitive characteristics of the MnO_2/CNxNTs/CC composite electrodes are a promising material for supercapacitors. The charge/discharge behavior of MnO_2/CNxNTs/CC composite electrode at different current densities was examined, as shown in Figure 8(a). From the charge and discharge process, the linear and symmetrical curves, at various operated current densities, illustrated the features of high columbic efficiency and lower equivalent series resistance. The cycling lifetime of the MnO_2/CNxNTs/CC composite electrode was also investigated, at a current density of 0.84 A g^{-1} in 0.1 M Na_2SO_4 medium. As shown in Figure 8(b), the gravimetric capacitance decreased by 7% during the first 250 cycles, and remained almost constant during the entire 2,000 cycles. The possible reason for the decrease of capacitance may be because of the equilibration of the electrode potential. The coulomb efficiency, which is the ratio of charge capacitance and discharge capacitance, demonstrates retention of more than 98% during the cycling process, as shown in Figure 8(b). Hence, these capacitive natures of MnO_2/CNxNTs/CC electrode can be attributed to the conformal coverage of nanostructured MnO_2, which facilitates the fast penetration of the electrolytes and the extraordinary electronic conductivity of CNxNTs to allow rapid electron-transfer for charge storage and delivery.

4. Conclusions

Uniform and conformal coverage of the MnO_2 thin layer successfully deposited onto hierarchical current collector of direct-grown CNxNTs on CC by using a simple and cost-effective spontaneous reduction method at room temperature. The N incorporation in CNTs significantly affects not only the creation of surface defects, which act as anchoring sites, but also the function of electron donors, to further reduce the work function of CNxNTs in facilitating the

spontaneous reduction of MnO_4^- to MnO_2. The hierarchical electrode of MnO_2/CNxNTs/CC benefits the effective utilization of MnO_2 thin layer and the superior conductivity of CNxNTs for electron path. The specific capacitance of MnO_2/CNxNTs/CC composite electrode can be as high as 589.1 Fg^{-1}, which is higher than those reported in prior studies. The excellent cycle lifetime of over 2,000 cycles of galvanostatic charge/discharge process demonstrates the MnO_2/CNxNTs/CC as a promising active material for a large-scale, flexible, and electrochemically stable supercapacitor.

Acknowledgments

This paper was financially supported by the Ministry of Education, Asian Office of Aerospace Research and Development under AFOSR, National Science Council, National Taiwan University, and Academia Sinica, Taiwan.

References

[1] B. E. Conway, *Electrochemical Supercapacitors, Scientific Fundamentals and Technological Applications*, Kluwer Academic/Plenum Press, New York, NY, USA, 1999.

[2] B. E. Conway, "Transition from "supercapacitor" to "battery" behavior in electrochemical energy storage," *Journal of the Electrochemical Society*, vol. 138, no. 6, pp. 1539–1548, 1991.

[3] Y. K. Hsu, J. L. Yang, Y. G. Lin, S. Y. Chen, L. C. Chen, and K. H. Chen, "Electrophoretic deposition of PtRu nanoparticles on carbon nanotubes for methanol oxidation," *Diamond & Related Materials*, vol. 18, no. 2-3, pp. 557–562, 2009.

[4] V. L. Pushparaj, M. M. Shaijumon, A. Kumar et al., "Flexible energy storage devices based on nanocomposite paper," *Proceedings of the National Academy of Sciences of the United States of America*, vol. 104, no. 34, pp. 13574–13577, 2007.

[5] Y. Y. Horng, Y. C. Lu, Y. K. Hsu, C. C. Chen, L. C. Chen, and K. H. Chen, "Flexible supercapacitor based on polyaniline nanowires/carbon cloth with both high gravimetric and area-normalized capacitance," *Journal of Power Sources*, vol. 195, no. 13, pp. 4418–4422, 2010.

[6] Y. C. Chen, Y. K. Hsu, Y. G. Lin et al., "Highly flexible supercapacitors with manganese oxide nanosheet/carbon cloth electrode," *Electrochimica Acta*, vol. 56, no. 20, pp. 7124–7130, 2011.

[7] H. Zhang, G. Cao, and Y. Yang, "Carbon nanotube arrays and their composites for electrochemical capacitors and lithium-ion batteries," *Energy and Environmental Science*, vol. 2, no. 9, pp. 932–943, 2009.

[8] G. Lota, K. Fic, and E. Frackowiak, "Carbon nanotubes and their composites in electrochemical applications," *Energy and Environmental Science*, vol. 4, pp. 1592–1605, 2011.

[9] P. Simon and Y. Gogotsi, "Materials for electrochemical capacitors," *Nature Materials*, vol. 7, no. 11, pp. 845–854, 2008.

[10] K. Naoi and P. Simon, "New materials and new configurations for advanced electrochemical capacitors," *Journal of the Electrochemical Society*, vol. 17, no. 6, pp. 34–37, 2008.

[11] C. C. Hu, K. H. Chang, M. C. Lin, and Y. T. Wu, "Design and tailoring of the nanotubular arrayed architecture of hydrous RuO2 for next generation supercapacitors," *Nano Letters*, vol. 6, no. 12, pp. 2690–2695, 2006.

[12] Y. G. Wang, H. Q. Li, and Y. Y. Xia, "Ordered whiskerlike polyaniline grown on the surface of mesoporous carbon and its electrochemical capacitance performance," *Advanced Materials*, vol. 18, no. 19, pp. 2619–2623, 2006.

[13] X. Zhang, W. Shi, J. Zhu et al., "High-power and high-energy-density flexible pseudocapacitor electrodes made from porous CuO nanobelts and single-walled carbon nanotubes," *ACS Nano*, vol. 5, no. 3, pp. 2013–2019, 2011.

[14] A. E. Fischer, K. A. Pettigrew, D. R. Rolison, R. M. Stroud, and J. W. Long, "Incorporation of homogeneous, nanoscale MnO_2 within ultraporous carbon structures via self-limiting electroless deposition: implications for electrochemical capacitors," *Nano Letters*, vol. 7, no. 2, pp. 281–286, 2007.

[15] H. Zhang, G. P. Cao, Z. Y. Wang, Y. S. Yang, Z. J. Shi, and Z. N. Gu, "Growth of manganese oxide nanoflowers on vertically-aligned carbon nanotube arrays for high-rate electrochemical capacitive energy storage," *Nano Letters*, vol. 8, no. 9, pp. 2664–2668, 2008.

[16] M. Toupin, T. Brousse, and D. Bélanger, "Influence of microstucture on the charge storage properties of chemically synthesized manganese dioxide," *Chemistry of Materials*, vol. 14, no. 9, pp. 3946–3952, 2002.

[17] O. Ghodbane, J. L. Pascal, and F. Favier, "Microstructural effects on charge-storage properties in MnO_2-based electrochemical supercapacitors," *ACS Applied Materials and Interfaces*, vol. 1, no. 2, pp. 1130–1139, 2009.

[18] DOI/USGS, "Rare earth elements—critical resources for high technology," Fact Sheet 087-02, 2002.

[19] Y. K. Hsu, Y. C. Chen, Y. G. Lin, L. C. Chen, and K. H. Chen, "Reversible phase transformation of MnO_2 nanosheets in an electrochemical capacitor investigated by in situ Raman spectroscopy," *Chemical Communications*, vol. 47, no. 2, pp. 1252–1254, 2011.

[20] C. C. Hu, C. Y. Hung, K. H. Chang, and Y. L. Yang, "A hierarchical nanostructure consisting of amorphous MnO_2, Mn_3O_4 nanocrystallites, and single-crystalline MnOOH nanowires for supercapacitors," *Journal of Power Sources*, vol. 196, no. 2, pp. 847–850, 2011.

[21] W. C. Fang, K. H. Chen, and L. C. Chen, "Superior capacitive property of RuO_2 nanoparticles on carbon nanotubes incorporated with nitrogen," *Nanotechnology*, vol. 18, no. 48, Article ID 485716, 2007.

[22] C. L. Sun, Y. K. Hsu, Y. G. Lin et al., "Ternary PtRuNi nanocatalysts supported on N-doped carbon nanotubes: deposition process, material characterization, and electrochemistry," *Journal of the Electrochemical Society*, vol. 156, no. 10, pp. B1249–B1252, 2009.

[23] L. C. Chen, C. Y. Wen, C. H. Liang et al., "Controlling steps during early stages of the aligned growth of carbon nanotubes using microwave plasma enhanced chemical vapor deposition," *Advanced Functional Materials*, vol. 12, no. 10, pp. 687–692, 2002.

[24] S. B. Ma, K. Y. Ahn, E. S. Lee, K. H. Oh, and K. B. Kim, "Synthesis and characterization of manganese dioxide spontaneously coated on carbon nanotubes," *Carbon*, vol. 45, no. 2, pp. 375–382, 2007.

[25] W. C. Fang, J. H. Huang, L. C. Chen, Y. O. Su, K. H. Chen, and C. L. Sun, "Carbon nanotubes grown directly on ti electrodes and enhancement of their electrochemical properties by nitric acid treatment," *Electrochemical and Solid-State Letters*, vol. 9, no. 1, pp. A5–A8, 2006.

[26] D. G. McCulloch, S. Prawer, and A. Hoffman, "Structural investigation of xenon-ion-beam-irradiated glassy carbon," *Physical Review B*, vol. 50, no. 9, pp. 5905–5917, 1994.

[27] Y. G. Lin, Y. K. Hsu, J. L. Yang, S. Y. Chen, K. H. Chen, and L. C. Chen, "Effects of nitrogen-doping on the microstructure,

bonding and electrochemical activity of carbon nanotubes," *Diamond & Related Materials*, vol. 18, no. 2-3, pp. 433–437, 2009.

[28] H. C. Choi, M. Shim, S. Bangsaruntip, and H. Dai, "Spontaneous reduction of metal ions on the sidewalls of carbon nanotubes," *Journal of the American Chemical Society*, vol. 124, no. 31, pp. 9058–9059, 2002.

[29] R. Czerw, M. Terrones, J. C. Charler et al., "Identification of electron donor states in n-doped carbon nanotubes," *Nano Letters*, vol. 1, no. 9, pp. 457–460, 2001.

[30] C. L. Sun, H. W. Wang, M. Hayashi, L. C. Chen, and K. H. Chen, "Atomic-scale deformation in N-doped carbon nanotubes," *Journal of the American Chemical Society*, vol. 128, no. 26, pp. 8368–8369, 2006.

[31] C. M. Julien, M. Massot, and C. Poinsignon, "Lattice vibrations of manganese oxides: part I. Periodic structures," *Spectrochimica Acta Part A*, vol. 60, no. 3, pp. 689–700, 2004.

[32] W. C. Fang, M. S. Leu, K. H. Chen, L. C. Chen, and J. H. Chen, "Effect of structural morphology on electrochemical properties of carbon nanotubes directly grown on Ti foil," *Electrochemical and Solid-State Letters*, vol. 10, no. 11, pp. K60–K62, 2007.

[33] Q. B. Wen, L. Qiao, W. T. Zheng et al., "Theoretical investigation on different effects of nitrogen and boron substitutional impurities on the structures and field emission properties for carbon nanotubes," *Physica E*, vol. 40, no. 4, pp. 890–893, 2008.

[34] C. C. Hu, H. Y. Guo, K. H. Chang, and C. C. Huang, "Anodic composite deposition of $RuO_2 \cdot xH_2O$-TiO_2 for electrochemical supercapacitors," *Electrochemistry Communications*, vol. 11, no. 8, pp. 1631–1634, 2009.